ONLINE FIRST

This is a provisional PDF only. Copyedited and fully formatted versión will be made available at final publication

HISTOLOGY AND HISTOPATHOLOGY

ISSN: 0213-3911
e-ISSN: 1699-5848

Persistent mdx diaphragm alterations are accompanied by increased expression and activity of calcium and muscle-specific proteins

Authors: Rhayanna B. Gaglianone, Flavia Fonseca Bloise, Jussara Lagrota-Candido, Claudia Mermelstein and Thereza Quirico-Santos

DOI: 10.14670/HH-18-334
Article type: ORIGINAL ARTICLE
Accepted: 2021-04-07
Epub ahead of print: 2021-04-07

Persistent mdx diaphragm alterations are accompanied by increased expression and activity of calcium and muscle-specific proteins

Rhayanna B. Gaglianone[a,b], Flavia Fonseca Bloise[c], Jussara Lagrota-Candido[a], Claudia Mermelstein[b*], Thereza Quirico-Santos[a]

[a] Instituto de Biologia, Universidade Federal Fluminense, Niterói, RJ, Brazil

[b] Instituto de Ciências Biomédicas, Universidade Federal do Rio de Janeiro, Rio de Janeiro, RJ, Brazil

[c] Instituto de Biofísica Carlos Chagas Filho, Universidade Federal do Rio de Janeiro, Rio de Janeiro, RJ, Brazil

Rhayanna B. Gaglianone: rgaglianone@id.uff.br ORCID: 0000-0001-9673-3986

Flavia Fonseca Bloise: flaviabloise@biof.ufrj.br ORCID: 0000-0002-5207-2896

Jussara Lagrota-Candido: jlagrota@id.uff.br ORCID: 0000-0002-6573-561X

Claudia Mermelstein: mermelstein@ufrj.br ORCID: 0000-0002-8897-8526

Thereza Quirico-Santos: tquirico@id.uff.br ORCID: 0000-0003-0501-8720

*Corresponding author

E-mail: mermelstein@ufrj.br

Abstract

The mdx mouse model of Duchenne Muscular Dystrophy (DMD) presents sarcolemma instability and develops a mild multi-stage dystrophinopathy characterized by intense myonecrosis with inflammatory infiltrate at 4-weeks; muscular regeneration at 12-weeks and persistent fibrosis onwards. Mdx diaphragm muscle has a more severe phenotype with structural and functional deterioration that closely resembles the diaphragm impairment responsible for DMD human patients' morbidity. Herein, we compared calcium deposits, activity of calcium-related proteases, and expression of muscle-specific proteins in mdx diaphragm at 4-weeks and 12-weeks. We found increased calcium deposits mainly at 12-weeks, concomitant with high activity of calpains and matrix metaloprotease-9, but decreased expression of *Myhc4* (Myhc IIb) and *Atpa2a1* (SERCA1), and high expression of the myogenic regulatory factors *Myod1* and *Myog*. Our results suggest that increased calcium deposits and persistent activity of calcium dependent proteases throughout the disease are involved in the degeneration and regeneration processes in the mdx diaphragm.

Keywords: mdx mouse; muscular dystrophy; diaphragm; calpain; calcium

1-Introduction

Duchenne muscular dystrophy (DMD) is an X-linked fatal disease caused by the lack of dystrophin, an important structural protein that connects the actin cytoskeleton to components of the extracellular matrix (ECM) (Allen et al., 2016). Although the loss of patient ambulation correlates to progressive degeneration and weakening of limb muscles, the leading cause of morbidity and mortality is progressive cardiorespiratory failure due to impairment of diaphragm functioning. The diaphragm muscle is highly susceptible to contraction-mediated injury being affected earlier and more severely than other skeletal muscles due to malfunction and degeneration, which predisposes to myonecrosis and excessive proliferation of connective tissue (Manning and O'Malley, 2015). The dystrophin-deficient mdx mouse develops a mild DMD phenotype with distinct histological features of muscle damage related to myonecrosis (3 and 4w), regeneration (12w), and later loss of functional contractile myofibers due to exhaustion of regenerative capacity (Manning and O'Malley, 2015; McGreevy et al., 2015). Muscle damage is highly dependent upon chronic contractile activity which partly explains why respiratory muscles are more affected than limb muscles. Mdx diaphragm undergoes extensive myonecrosis with structural and functional deterioration similar to human pathology (Allen et al., 2016; McRae et al., 2020).

Calcium metabolism is responsible for regulating many cellular events and is especially important for both degeneration and regeneration processes, particularly in DMD muscles (Allen et al., 2016; Tu et al., 2016). Interestingly, the mdx EDL muscle shows high calcium deposits and a reduction in mitochondrial activity at the peak of regeneration (12w) (Gaglianone et al., 2019). Calcium proteases, like matrix metalloproteases (MMP) and calpains (CAPN) participate in a variety of cellular events (Goll et al., 2003; Bozzi et al., 2015; Allen et al., 2016). Gelatinases MMP2 and MMP9

are responsible for cleaving ECM components and for regulating processes such as regeneration, motility and differentiation of skeletal muscle fibers. MMP2 is particularly important for the growth of regenerated myofibers whereas MMP9 mainly for ECM degradation (Miyazaki et al., 2011; Shiba et al., 2015). CAPN1 and CAPN2 are cytosolic enzymes responsible for maintaining myofibrils that share the same substrates but differ in their calcium concentration for activation. Calpains are often related to the pathogenesis of various diseases, with CAPN1 and CAPN2 being considered essential for muscle repair and resealing of the plasma membrane by eccentric skeletal muscle injury (Potz et al., 2016; Piper et al., 2020). The already described presence of increased amounts of calcium and calcium-related proteins in mdx limb muscles (Gaglianone et al., 2019) led us to analyze the calcium deposits and calcium-related proteins in the diaphragm muscle of mdx mice.

2-Material and methods

2.1-Ethics statement

This study followed the principles of good laboratory animal care and experimentation in compliance with ethical recommendations in the guidelines of the Brazilian College for Animal Experimentation. The study protocol for handling of animals was approved by the Institutional Animal Care Committee of Universidade Federal Fluminense (protocol CEUA 00174/09).

2.2-Animals

Isogenic male *mdx* (C57BL/10ScSn-Dmdmdx/J) dystrophic and age-matched C57BL/10J (C57) control non-dystrophic mice at 4 and 12-weeks (w) of age were kept in the animal housing facilities at the Department of Immunobiology in the Universidade Federal Fluminense. Mice were housed in a ventilated rack (Alesco, Brazil) in autoclaved cages and kept at a constant 12 h/12 h light-dark cycle and temperature (24ºC) with free access to food and water. Mice were euthanized by cervical dislocation, and the diaphragm muscle was collected. The animals were euthanized at the ages of 4 and 12w. The number of animals used for each experimental condition (C57 4w, C57 12w, mdx 4w, and mdx 12w) was: 5 for Alizarin Red staining, 6 for zymography, and 5 for qPCR.

2.3-Tissue processing

Whole diaphragm muscle from C57BL10 and mdx mice were collected, weighed and macerated individually (1/10 w/v) in a specific lysis buffer for metalloproteases (100mM Tris-HCl, pH 7,6, 200mM NaCl, 100mM $CaCl_2$, 1% (v/v) Triton X-100) (Gaglianone et al., 2020) and for calpains (50mM HEPES, pH 7.6, 150mM NaCl, 10%

(v/v) glycerol, 0.1% (v/v) Triton X-100, 5mM EDTA, 10mM 2-mercaptoethanol, 100µM PMSF, 10 µg/mL leupeptin) (Arthur and Mykles, 2000). All muscles were mashed in an ice-bath until total dissociation on the same day of dissection using TissueRuptor (Qiagen, USA). Tissue extracts were centrifuged for 15 min under 15,000 x*g* at 4ºC and the supernatant was recovered, stored until use in multiple aliquots at -20ºC. Protein concentration was quantified by Lowry method. For Alizarin red staining, diaphragm muscles were fixed in 10% formalin for 18 hours and processed into paraffin-embedded blocks.

2.4-Alizarin Red S staining for calcium deposits analysis

Muscles from C57BL10 and *mdx* mice were fixed in 10% neutral buffered formalin and further processed into paraffin-embedded cassettes. Sections of 5-µm -thickness were placed on poly-lysine coated-slides. Muscle sections were stained with Alizarin Red S 2% (ARS) solution for 3 to 5 minutes and dehydrated in acetone, acetone-xylol (1:1), and xylol, for 20 seconds each step and mounted in glycerol. Images of calcium deposits birefringence were observed and acquired under bright-field and polarization on an Axiovert 100 microscope (Zeiss, Germany). Calcium deposits were quantified under polarized light microscopy, a contrast-enhancing technique that improves the quality of the image of birefringent materials, such as calcium deposits (Gaglianone et al. 2020).

2.5-Casein zymography assay for CAPN activity

Casein gels for calpain activity were performed as described previously (Arthur and Mykles 2000). Gels consisted of 10% (w/v) polyacrylamide impregnated with casein 10mg/mL (Sigma), and 5% (w/v) polyacrylamide for stacking gels and 40µg of protein

was loaded in each gel lane. Gels were run (Power Pac 200, Bio-Rad, USA) with electrophoresis buffer (25mM Tris base, 125mM glycine, 1mM EDTA, pH 8.0 and 10mM 2-mercaptoethanol) at 125 Volts. Gels were removed and washed twice for 30 minutes each with the incubation buffer (50mM Tris-HCl, pH 7.0, 5mM $CaCl_2$, 10mM 2-Mercaptoethanol) under gentle swirling. Thereafter, gels were transferred to a new incubation buffer and incubated overnight at room temperature under gentle swirling. Three distinguishable bands are evident: the first one refers to CAPN1, the second band to CAPN2, and the third band to autolyzed calpain (Aut CAPN), which could be generated from either CAPN1 or CAPN2. The autolysis process occurs in the tissue, prior to gel loading (Goll et al., 2003; Arthur and Mykles, 2000).

2.6-Gene expression

Total RNA from diaphragm was extracted using the TRIzol Reagent (Invitrogen, USA) and Nucleo Spin RNA® (Macherey Nagel, Denmark). Briefly, the aqueous phase from the initial TRIzol protocol was placed into the Machery Nagel Nucleo Spin RNA column and followed downstream according to the manufacturer's protocols. The cDNA synthesis was performed using the High-Capacity cDNA Reverse Transcription Kit (Applied Biosystems, USA) according to the manufacturer's protocols using 1000 ng of total RNA. Following cDNA synthesis, mRNA expressions were evaluated by qPCR using the HOT FIREPol® Evagreen® qPCR Supermix (Solis Biodyne, Denmark) using the Master Cycler Realplex system (Eppendorf, Germany). Primer pairs' sequences are shown in Table 1. Quantification of mRNA expression was calculated from the standard curve method and corrected expression by the geometric mean of the reference genes: *Rpl0*, *Hprt1*. The best reference gene combinations were chosen according to their Cq values, using the minor variance between the groups. PCR

program was as follows: denaturation 12 min 95°C, 40 cycles of 15 sec 95°C, 30 sec 60°C, 30 sec 72°C, following melting program. qPCR quality and genomic DNA contamination was checked using intron-spanning primers, reverse transcriptase-negative samples from cDNA synthesis and melting curve analysis obtained from each reaction.

2.7-Gelatin zymography assay for matrix metalloprotease activity

SDS-PAGE zymogram gels consisted of 7.5% polyacrylamide-SDS impregnated with 2 mg/mL type A gelatin from porcine skin (Sigma) and 4% polyacrylamide-SDS for stacking gels. 40µg of protein was loaded in each gel lane. Gels were further washed twice for 30 min in 2.5% Triton X-100 solution, and then incubated at 37°C for 24h in substrate buffer (10mM Tris–HCl buffer, pH 7.5 with 5mM $CaCl_2$, 1µM $ZnCl_2$). The MMP electrophoresis was performed in the presence of SDS, during the washing process with renaturation buffer (Triton X-100 2.5%), the SDS is removed which activates the enzyme without the inhibitory pro-peptide removal, allowing the identification of inactive enzyme (Gaglianone et al., 2020).

2.8-Gel staining

Calpain and MMP gels were stained with stain solution [0.25% (w/v) Coomassie blue, 40% (w/v) methanol, 7% (w/v) acetic acid] and washed with discoloration solution [50% (w/v) methanol, 10% (w/v) acetic acid] until bands were visible. The zymogram bands for casein or gelatin appear as a bright, clear zone on a dark background, but the images were reversed for easy viewing. Both gels from 4w and 12w were prepared and run together in the same conditions, thus allowing comparison between the two ages.

2.9-Image acquisition and quantification

Zymogram images were acquired using the software L-Pix (Loccus-Brazil) and gel bands quantified by LabImage (Loccus-Brazil). Quantification of the area occupied by calcium deposits from Alizarin Red S staining was performed using Image J software.

2.10-Statistical analysis

Data were analyzed with GraphPad Prism™ 7.0 (GraphPad Software Inc. San Diego, CA, USA), and for statistical significance t-test non-paired and non-parametric Mann-Whitney test were used. The results were expressed as mean ± standard deviation (SD). A p-value < 0.05 was considered statistically significant. Outliers were detected by Grubb's test and removed from the data analysis.

3-Results

3.1-Calcium deposits are increased in mdx diaphragm

Membrane injury, an early event in DMD muscular dystrophy causes an increase in calcium influx (Allen et al., 2016). We assessed calcium deposits using Alizarin Red S (ARS), a stain that binds specifically to calcium ions, forming birefringent deposits that can be visualized under polarized light. Microscopy analysis (Fig. 1A) evidenced low amounts of calcium deposits in the C57 diaphragm at 12w, but calcium deposits were not detected in C57 with 4w. In contrast, intense calcium deposits were found in mdx diaphragm at 4w and 12w (arrow, Fig. 1A). Alizarin Red S staining was detected mainly in mdx muscle fibers undergoing myonecrosis and at the extracellular space between muscle fibers (Fig. 1). Quantification (Fig. 1B) of the mdx diaphragm showed increased amounts of calcium deposition corresponding to 4% of the total area at 4w and 9.3% at 12w. Furthermore, mdx diaphragm at 12w had 4.5-fold more calcium than non-dystrophic control and 1.4-fold more calcium than mdx at 4w.

3.2-Diaphragm presents elevated activity of calpains

Next, we evaluated the activity of enzymes that are modulated by calcium. Casein zymogram identified three distinct bands (Fig. 2A) corresponding to CAPN1, CAPN2, and the autolyzed (Aut) CAPN (Arthur and Mykles 2000; Goll et al. 2003; Pomponio et al. 2008). Quantification of the bands (Fig. 2B-D) showed a decrease of CAPN1 activity (Fig. 2B) in the mdx diaphragm at both 4 and 12w, while CAPN2 (Fig. 2C) seemed elevated in mdx at 4w, but not at 12w. The intense decrease of CAPN1 coincided with the appearance of the autolyzed CAPN (Fig. 2A). Autolyzed CAPN (Fig. 2D) was detected exclusively in the mdx at 4w, while at 12w it was detected in both C57 and mdx, but mdx 12w presented 7-fold more activity than C57 at 12w. The activity of Aut

CAPN was 1.7-fold higher in mdx at 12w when compared to mdx at 4w, thus suggesting a role for calpains in mdx diaphragm during the regeneration phase.

We further analyzed the expression of *Capn1* and *Capn2* (Fig. 2E-H) by real-time PCR (qPCR) to find out any alterations at the transcriptional level. Interestingly, we found no difference between mdx and C57 mice at both 4w (Fig. 2E-F) and 12w (Fig. 2G-H) for *Capn1* and *Capn2* gene expression. Such results suggest that the dystrophic diaphragm environment activates calpains by post-translational mechanisms.

3.3-Diaphragm down-expresses fast fatigable fibers

Due to increased calcium deposits in mdx diaphragm we decided to analyze the expression of calcium-dependent proteins necessary for muscle maintenance. Hence, we evaluated the gene expression of *Myhc7, Myhc2, Myhc1, Myhc4, Atpa1*, *Atpa2a,* related to slow fiber type I, fast fibers type IIa, IIx, IIb, SERCA1 and SERCA2a, respectively. Analysis of the expression of *Myhc* (Fig. 3A-B) showed a significant reduction of *Myhc4* (MyHC IIb) in the mdx at 4w and 12w, but no differences were found in the expression of *Myhc7, Myhc2, Myhc1* (MyHC I, IIa, and IIx). The expression of *Atpa1* (SERCA1) (Fig. 3C-D) showed a prominent decrease in the mdx at 12w but not at 4w, and no difference was observed for *Atpa2a* (SERCA2a) (Fig. 3E-F) at either age.

3.4-Dystrophic diaphragm displays intense extracellular matrix alterations

We also analyzed the activity of calcium-dependent matrix metalloproteases (MMP) -2 and -9. MMP zymograms (Fig. 4A) showed four distinct bands related to MMP9, pre proMMP2, proMMP2 (zymogenic forms of MMP2) and active MMP2, respectively. Quantification of the bands showed increased activity of MMP2 zymogenic forms (Fig. 4B-C) specifically in mdx diaphragm at 12w when compared to age-matched C57, but

no differences were observed between mdx at 4 and 12w. Active MMP2 (Fig. 4D) and MMP9 (Fig. 4E) were found exclusively in mdx mice. Active MMP2 was increased at 4w and decreased at 12w, while the MMP9 was elevated at both 4w and 12w. Interestingly, no significant differences were found in the activity of MMP9 between mdx at 4w and mdx at 12w (Fig. 4E).

We further evaluated the expression of two myogenic regulatory factors *Myod1* and *Myogenin* genes (Fig. 4F-I) to check their possible relationship with mdx diaphragm pathology. We observed a marked increase in the expression of *Myod1* (Fig. 4F-G) and *Myogenin* (Fig. 4H-I) in mdx at 4w and 12w when compared to age-matched C57. Since MyoD1 and myogenin are involved in proliferation and differentiation of muscle cells, these results suggest that mdx diaphragm is undergoing constant muscle regeneration.

4-Discussion

The mdx mouse is the suitable murine animal model for studying the pathophysiology of DMD. Unlike the human homologue that presents progressive degeneration, the mdx displays an age-dependent pathology on limb-muscles characterized by extensive myonecrosis at 4w, increased regeneration at 12w, but fibrosis with fatty tissue deposition and loss of functional contractile myofibers at 24 weeks due to exhaustion of regenerative capacity (McGreevy et al., 2015; Grounds et al., 2020). The mdx mice compensate the lack of dystrophin probably by efficient myofiber type reorganization, expression of smaller forms of dystrophin and reactivation of utrophin expression, the embryonic form of dystrophin (Selsby et al., 2012; Pigozzo et al., 2013). In contrast, the mdx diaphragm presents intense myonecrosis with an auto-amplifying pro-inflammatory cytokine production that resembles the severity of DMD patients (Gama et al., 2020). Furthermore, Burns and colleagues (2019b) suggest that the progressive decline in ventilatory performance in mdx relates to the loss of compensation provided by accessory muscles of breathing.

The dystrophic cells present membrane tearing caused by stretch-induced injury which is the main non-regulated calcium entry (Allen et al., 2016). We have previously reported intense calcium deposits in limb-muscles, especially in the homogeneous fast-twitch muscle EDL at 12w and reduced mitochondrial activity (Gaglianone et al., 2019). We considered it important to analyze calcium deposits in the mdx diaphragm muscle, which presents a continuous tissue degeneration associated with inflammation, oxidative stress, and fibrosis (Burns et al., 2019a). Calcium deposits were found almost exclusively in the mdx at both 4w and 12w, as compared to control C57. But mdx at 12w had 1.4 times more calcium than at 4w, thus suggesting an important role for calcium in both myonecrosis and muscle regeneration. Low calcium deposits in C57

mice at 12w may be attributed to stress induced by constant breathing movement of respiration. Calcium is responsible for the activation of calcium-dependent enzymes, such as CAPN1 and CAPN2 that undergo an autoproteolytic cleavage during activation, generating the autolyzed CAPN (Goll et al., 2003). The autolyzed CAPN was elevated in mdx diaphragm with higher content especially at 12w thus suggesting the importance of calpains during muscle regeneration. The presence of autolyzed CAPN in the control non-dystrophic mouse at 12w could be due to extensive and continuous use of the diaphragm as a vital respiratory muscle (Lessa et al., 2016). Despite the increased activity of calpains, we did not find an alteration in *Capn1* and *Capn2* expression, suggesting that the high CAPN activity could be due to a post-translational mechanism induced by the dystrophic environment.

Muscle tissue presents two main isoforms of the calcium-related enzyme SERCA: SERCA1 that has a faster kinetic, and SERCA2a with a slower kinetic (Schiaffino and Reggiani, 2011). These proteins are strictly fiber-type dependent and are co-expressed with the myosin heavy chain (MyHC) isoforms. SERCA1 is co-expressed with the fast MyHC IIb, IIx and IIa but the density of SERCA1 is higher in fiber type IIb than in type IIa whereas SERCA2a is co-expressed with MyHC I (Schiaffino and Reggiani, 2011; Tanihata and Takeda, 2016). Interestingly, unlike the previous report (Shavlakadze et al., 2004) that showed an increase of MyHC IIb fibers in the diaphragm muscle of mdx mice at 12w, we observed a marked decrease in the *Myhc4* expression in the fast MyHCIIb fibers at 4w and 12w and *SERCA1* expression in the mdx diaphragm at 12w. In accordance with our results, Burns and colleagues (2018) showed that the expression of MyHCIIb fibers was significantly reduced in diaphragm muscle from mdx mice, compared with wild type diaphragm.

Persistent tissue alteration is associated with increased pre-proMMP2 and proMMP2 zymogenic activities in the mdx diaphragm at 4w and 12w compared to age matched C57. The active MMP2 form was found exclusively in the mdx but we noticed a reduction of MMP2 activity especially during the regeneration phase (12w). High MMP9 activity solely in the mdx diaphragm (and not in C57) at both ages (4w and 12w) suggests an important role for MMP9 in the regulation of mdx diaphragm tissue alterations. Remarkably, our data showed no significant differences in the activity of MMP9 between mdx diaphragm at 4w and 12w, despite the reported role of MMP9 at later stages of mdx disease. It has been described that MMP-9 has multiple functions during mdx disease progression (Shiba et al., 2015), among the most relevant are the degradation of ECM components, such as collagen, and the proteolytic processing of latent TGF-β into an active form (Li et al., 2009). We hypothesize that while the activity of MMP9 does not change during mdx disease, its role could be quite different at early and late stages of the pathology, with a more prominent ECM degradation role at the beginning of the disease and a TGF-β-related action at later stages. Further experiments are required to address the role of MMP9 during mdx diaphragm development.

The collection of our results shows an increase (i) in calcium deposits, (ii) in the activity of the autolyzed form of CAPN, and (iii) in the activity of MMP2 and MMP9, in the mdx diaphragm at both 4w and 12w. These results point to a role of calcium and calcium-related enzymes in the mdx muscle pathology. The increase in calcium can activate different signaling pathways in the mdx respiratory muscle, since calcium is a pleiotropic ion which can bind and activate several calcium-binding proteins, including kinases, phosphatases, and transcription factors, in a cell specific manner. Thus, more studies are necessary to unravel the role of calcium in different signaling pathways and networks in the mdx diaphragm muscle.

Compliance with Ethical Statements

Conflict of Interest

The authors declare that they have no conflicts of interest concerning this article.

Funding

This study was supported by Fundação Carlos Chagas Filho de Apoio à Pesquisa do Estado do Rio de Janeiro (FAPERJ), Conselho Nacional de Desenvolvimento Científico e Tecnológico (CNPq) and Coordenação de Aperfeiçoamento de Pessoal de Nível Superior (CAPES).

Ethical approval

All applicable international, national, and/or institutional guidelines for the care and use of animals were followed. The study protocol for handling of animals was approved by the Institutional Animal Care Committee of Universidade Federal Fluminense (protocol CEUA 00174/09).

References

Allen D.G., Whitehead N.P. and Froehner S.C. (2016). Absence of dystrophin disrupts skeletal muscle signaling: roles of Ca2+, reactive oxygen species, and nitric oxide in the development of muscular dystrophy. Physiol. Rev. 96, 253-305.

Arthur J.S.C. and Mykles D.L. (2000). Calpain zymography with casein or fluorescein isothiocyanate casein in: Elce JS, Calpain methods and protocols, Springer Science & Business Media, pp. 109-116.

Bozzi M., Sciandra F. and Brancaccio A. (2015). Role of gelatinases in pathological and physiological processes involving the dystrophin–glycoprotein complex. Matrix Biol. 44, 130-137.

Burns D.P., Canavan L., Rowland J., O'Flaherty R., Brannock M., Drummond S.E., O'Malley D., Edge D. and O'Halloran K.D. (2018). Recovery of respiratory function in mdx mice co-treated with neutralizing interleukin-6 receptor antibodies and urocortin-2. J. Physiol. 596, 5175-5197.

Burns D.P., Drummond S.E., Bolger D., Coiscaud A., Murphy K.H., Edge D. and O'Halloran K.D. (2019a). N-acetylcysteine decreases fibrosis and increases force-generating capacity of mdx diaphragm. Antioxid. 8, 581.

Burns D.P., Murphy K.H., Lucking E.F. and O'Halloran K.D. (2019b). Inspiratory pressure-generating capacity is preserved during ventilatory and non-ventilatory behaviours in young dystrophic mdx mice despite profound diaphragm muscle weakness. J. Physiol. 597, 831-848.

Gaglianone R., Bloise F., Ortiga-Carvalho T., Quirico-Santos T., Costa M.L. and Mermelstein C. (2020). Comparative study of calcium and calcium-related enzymes with differentiation markers in different ages and muscle types in mdx mice. Histol. Histopathol. 35, 203-216.

Gaglianone R.B., Santos A.T., Bloise F.F., Ortiga-Carvalho T.M., Costa M.L., Quirico-Santos T., da Silva W.S. and Mermelstein C. (2019). Reduced mitochondrial respiration and increased calcium deposits in the EDL muscle, but not in soleus, from 12-week-old dystrophic mdx mice. Sci. Rep. 9, 1986.

Gama J.F., Pinheiro D.F., Da Silva R.F., Quirico-Santos T. and Lagrota-Candido J. (2020). The omentum harbors unique conditions in the peritoneal cavity to promote healing and regeneration for diaphragm muscle repair in mdx mice. Cell Tissue Res. 382, 447-455.

Goll D.E., Thompson V.F., Li H., Wei W. and Cong J. (2003). The calpain system. Physiol. Rev. 83, 731-801.

Grounds M.D., Terrill J.R., Al-Mshhdani B.A., Duong M.N., Radley-Crabb H.G. and Arthur P.G. (2020). Biomarkers for Duchenne muscular dystrophy: myonecrosis, inflammation and oxidative stress. Dis. Model Mech. 13.

Lessa T.B., de Abreu D.K., Bertassoli B.M. and Ambrósio C.E. (2016). Diaphragm: a vital respiratory muscle in mammals. Ann. Anat. 205, 122-127.

Li H., Mittal A., Makonchuk D.Y., Bhatnagar S. and Kumar A. (2009). Matrix metalloproteinase-9 inhibition ameliorates pathogenesis and improves skeletal muscle regeneration in muscular dystrophy. Hum. Mol. Genet. 18, 2584-2598.

Manning J. and O'Malley D. (2015). What has the mdx mouse model of duchenne muscular dystrophy contributed to our understanding of this disease?. J. Muscle Res. Cell Motil. 36, 155-167.

McGreevy J.W., Hakim C.H., McIntosh M.A. and Duan D. (2015). Animal models of Duchenne muscular dystrophy: from basic mechanisms to gene therapy. Dis. Model Mech. 8, 195-213.

McRae N.L., Addinsall A.B., Howlett K.F., McNeill B., McCulloch D.R. and Stupka N. (2020). Genetic reduction of the extracellular matrix protein versican attenuates inflammatory cell infiltration and improves contractile function in dystrophic mdx diaphragm muscles. Sci. Rep. 10, 1-19.

Miyazaki D., Nakamura A., Fukushima K., Yoshida K., Takeda S.I. and Ikeda S.I. (2011). Matrix metalloproteinase-2 ablation in dystrophin-deficient mdx muscle reduces angiogenesis resulting in impaired growth of regenerated muscle fibers. Hum. Mol. Genet. 20, 1787-1799.

Pigozzo S.R., Da Re L., Romualdi C., Mazzara P.G., Galletta E., Fletcher S., Wilton S.D. and Vitiello L. (2013). Revertant fibers in the mdx murine model of Duchenne muscular dystrophy: an age-and muscle-related reappraisal. PloS one 8, e72147.

Piper A.K., Sophocleous R.A., Ross S.E., Evesson F.J., Saleh O., Bournazos A., Yasa J., Reed C., Woolger N. and Sluyter R. (2020). Loss of calpains-1 and-2 prevents repair of plasma membrane scrape injuries, but not small pores, and induces a severe muscular dystrophy. Am. J. Physiol. Cell Physiol. 318, C1226-C1237.

Pomponio L., Lametsch R., Karlsson A.H., Costa L.N., Grossi A. and Ertbjerg P. (2008). Evidence for post-mortem m-calpain autolysis in porcine muscle. Meat Sci. 80, 761-764.

Potz B.A., Abid M.R. and Sellke F.W. (2016). Role of Calpain in Pathogenesis of Human Disease Processes, J. Nat. Sci. 2, e218.

Schiaffino S. and Reggiani C. (2011). Fiber types in mammalian skeletal muscles. Physiol. Rev. 91,1447-1531

Selsby J.T., Morine K.J., Pendrak K., Barton E.R. and Sweeney H.L. (2012). Rescue of dystrophic skeletal muscle by PGC-1α involves a fast to slow fiber type shift in the mdx mouse. PloS one 7, e30063.

Shavlakadze T., White J., Hoh J.F., Rosenthal N. and Grounds M.D. (2004). Targeted expression of insulin-like growth factor-I reduces early myofiber necrosis in dystrophic mdx mice. Mol. Ther. 10, 829-843.

Shiba N., Miyazaki D., Yoshizawa T., Fukushima K., Shiba Y., Inaba Y., Imamura M., Takeda S.I., Koike K. and Nakamura A. (2015). Differential roles of MMP-9 in early and late stages of dystrophic muscles in a mouse model of Duchenne muscular dystrophy. Biochim. Biophys. Acta Mol. Basis Dis. 1852, 2170-2182.

Tanihata J. and Takeda S.I. (2016). Changes in cytosolic Ca2+ dynamics in the sarcoplasmic reticulum associated with the pathology of Duchenne muscular dystrophy. J. Sports Med. Phys. Fitness 5, 309-312.

Tu M.K., Levin J.B., Hamilton A.M. and Borodinsky L.N. (2016). Calcium signaling in skeletal muscle development, maintenance and regeneration. Cell Calcium 59, 91-97.

Legends to figures

Legends to figures

Figure 1- Scattered Calcium deposits in the mdx diaphragm. A- Alizarin Red S (ARS) stain. B- Measurement of calcium deposition. Arrow- region of calcium cluster; white bar- C57; grey bar- mdx; n.d. - not detected; * $p<0.05$. Scale bar- 100 µm.

Figure 2- Detection of calpain activity by zymography and expression of *Capn1* and *Capn2* genes. A- Zymograms evidence the presence of calpains in C57 and in mdx diaphragm at 4 and 12w. Quantification of CAPN1 (B), CAPN2 (C) and autolyzed CAPN (D). n.s. - non-significant; n.d. - not detected; n= 3 to 6 mice. *Capn1* expression at 4w (E) and 12w (F). *Capn2* expression at 4w (G) and 12w (H). n=5 each. White bar- C57; grey bar- mdx; * $p<0.05$.

Figure 3- Expression of *Myhc, Atp2a1* and *Atpa2a* genes. A-B- Expression of *Myhc7, 2, 1, 4* (related to MyHC type I, IIa, IIx and IIb respectively) in mice at 4w and 12w. C-D- expression of *Atpa1* (SERCA1) at 4w and 12w. E-F expression of *Atpa2a* (SERCA2A) at 4w and 12w. n= 5; white bar- C57; grey bar- mdx; * $p<0.05$.

Figure 4- Activity of MMP2 and MMP9 and expression of *Myod1* and *Myog* genes. A- Zymograms show the presence of MMP9, pre-proMMP2, pro-MMP2 and active MMP2. Analysis of pre-pro MMP2 (B), pro-MMP2 (C), active MMP2 (D) and MMP9 (E). n= 3 to 6 each. F-G- Expression of *Myod1* in mice at 4w and 12w; H-I- Expression of *Myog* gene in mice at 4w and 12w; n= 5 each. White bar- C57; grey bar- mdx; n.d. - not detected; n.s. - non-significant; * $p<0.05$.

Gene	Primer sequences	GenBank accession
Rpl0	GGCCCTGCACTCTCGCTTTC TGCCAGGACGCGCTTGT	NM_007475.5
Hprt1	GCAGTACAGCCCCAAAATGG AACAAAGTCGGCCTGTATCCAA	NM_013556.2
Atp2a1	GGAATGCAGAGAACGCTATCG TCCTTTGCACTGACTTTCGGT	NM_007504.2 XM_006507268.1
Atp2a2	AATCTGACCCAGTGGCTGATG AGAGGGCTGGTAGATGTG TTG	NM_009722.3
Myh7	ACTGTCAACACTAAGAGGGTCA TTGGATGATTTGATCTTCCAGGG	NM_080728.3
Myh4	CACCTGGACGATGCTCTCAGA GCTCTTGCTCGGCCACTCT	NM_010855.3
Myh1	CGGAGTCAGGTGAATACTCACG GAGCATGAGCTAAGGCACTCT	NM_030679.2
Myh2	TGGAGGGTGAGGTAGAGAGTG TTGGATAGATTTGTGTTGGATTG	NM_001039545.2
Myog	TTGCTCAGCTCCCTCAACCAGGA TGCAGATTGTGGGCGTCTGTAGG	NM_031189.2
Myod1	GACCTGCGCTTTTTTGAGGACC CAGGCCCACAGCAAGCAGCGAC	NM_010866.2
Capn1	ATGACAGAGGAGTTAATCACCCC GCCCGAAGCGTTTCATAATCC	NM_001110504
Capn2	GGTCGCATGAGAGAGCCATC CCCCGAGTTTTGCTGGAGTA	NM_009794

Table 1- Primers sequences.

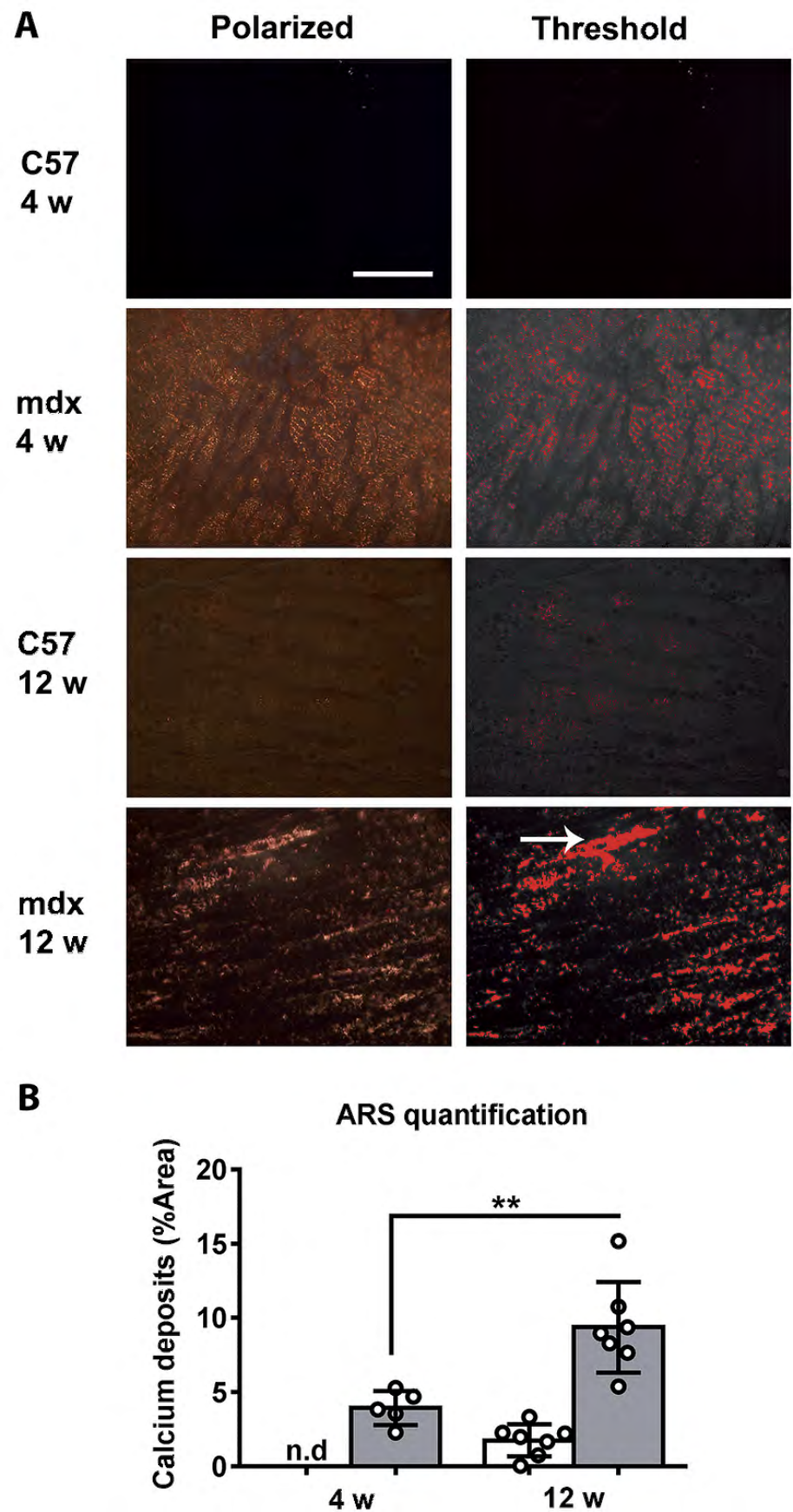
A
Polarized
Threshold
C57
4 w
mdx
4 w
C57
12 w
mdx
12 w
B
ARS quantification
Calcium deposits (%Area)
20
15
10
5
0
**
n.d
4 w
12 w

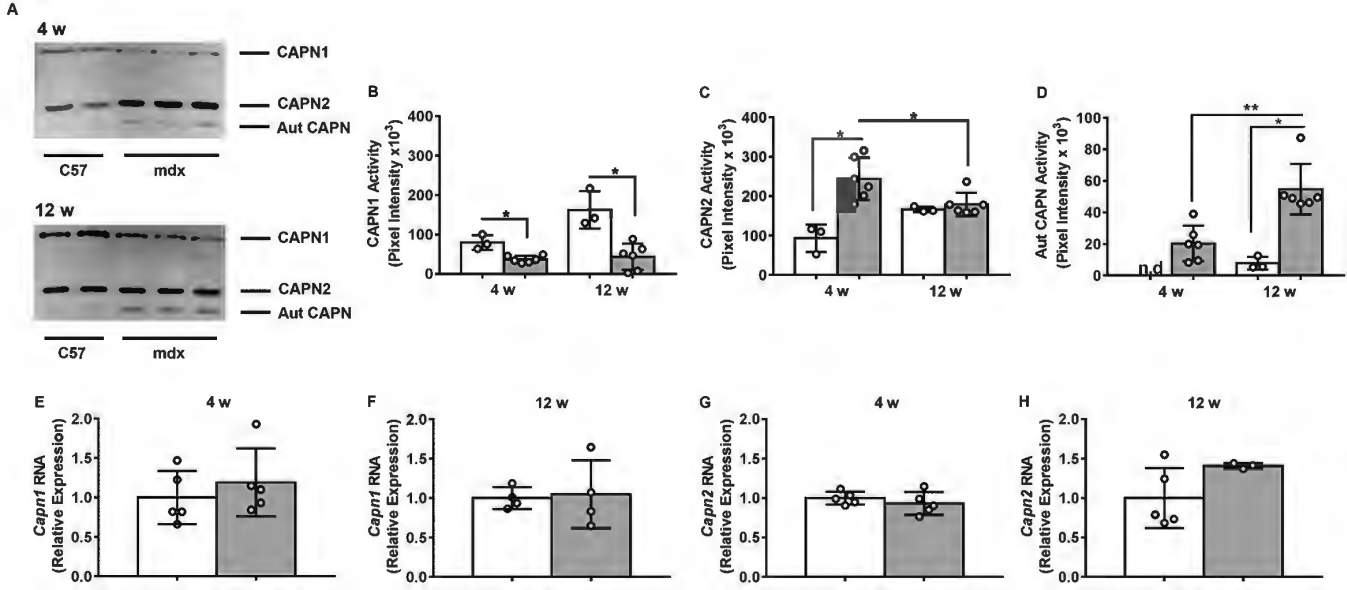
A
4 w
CAPN1
CAPN2
Aut CAPN
C57
mdx
12 w
CAPN1
CAPN2
Aut CAPN
C57
mdx
B
CAPN1 Activity
(Pixel Intensity x10³)
400
300
200
100
0
4 w
12 w
C
CAPN2 Activity
(Pixel Intensity x 10³)
400
300
200
100
0
4 w
12 w
D
Aut CAPN Activity
(Pixel Intensity x 10³)
100
80
60
40
20
0
n.d
4 w
12 w
E
4 w
Capn1 RNA
(Relative Expression)
2.0
1.5
1.0
0.5
0.0
F
12 w
Capn1 RNA
(Relative Expression)
2.0
1.5
1.0
0.5
0.0
G
4 w
Capn2 RNA
(Relative Expression)
2.0
1.5
1.0
0.5
0.0
H
12 w
Capn2 RNA
(Relative Expression)
2.0
1.5
1.0
0.5
0.0

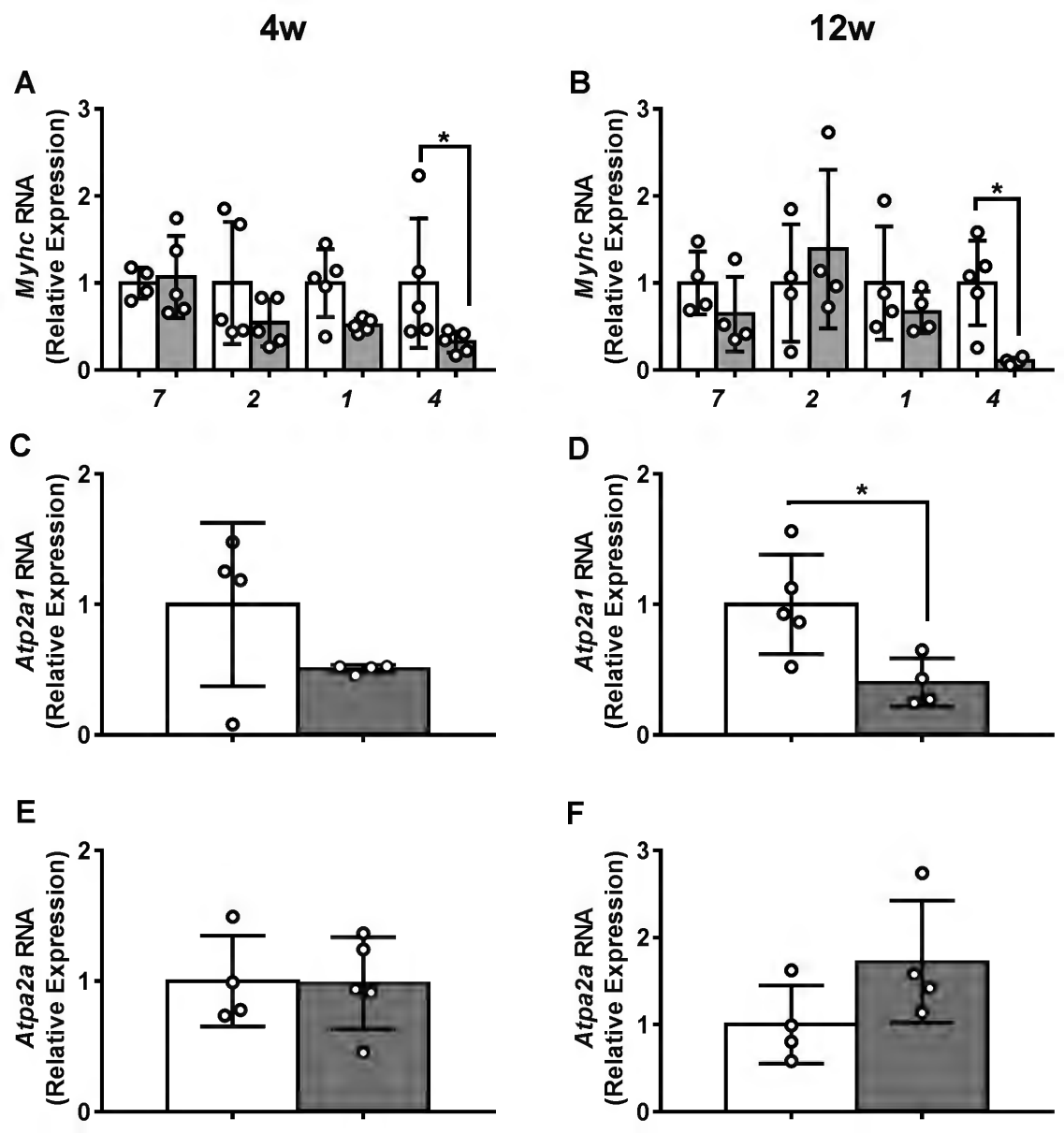
4w
12w
A
B
C
D
E
F
Myhc RNA (Relative Expression)
Atp2a1 RNA (Relative Expression)
Atpa2a RNA (Relative Expression)
7
2
1
4
*

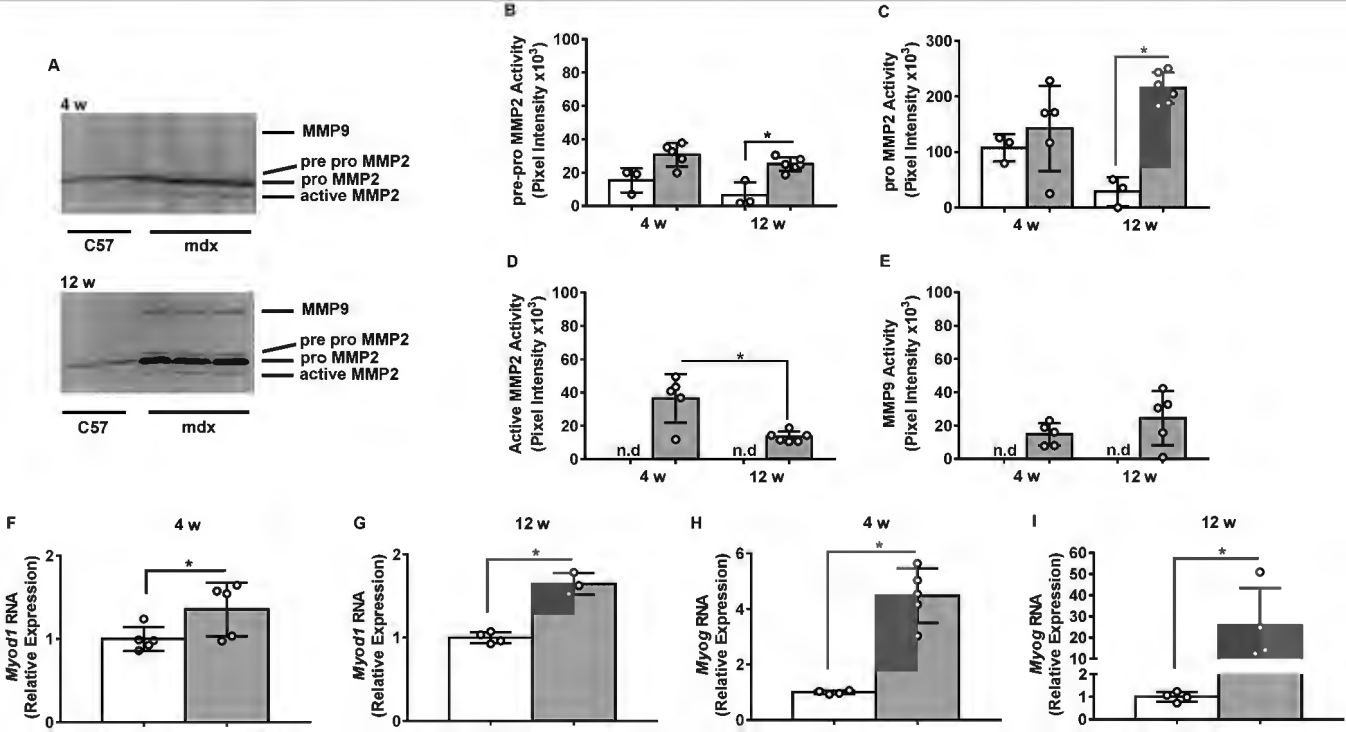
A
4 w
MMP9
pre pro MMP2
pro MMP2
active MMP2
C57
mdx
12 w
MMP9
pre pro MMP2
pro MMP2
active MMP2
C57
mdx
B
pre-pro MMP2 Activity (Pixel Intensity x10³)
4 w
12 w
C
pro MMP2 Activity (Pixel Intensity x10³)
4 w
12 w
D
Active MMP2 Activity (Pixel Intensity x10³)
n.d
n.d
4 w
12 w
E
MMP9 Activity (Pixel Intensity x10³)
n.d
n.d
4 w
12 w
F
4 w
Myod1 RNA (Relative Expression)
G
12 w
Myod1 RNA (Relative Expression)
H
4 w
Myog RNA (Relative Expression)
I
12 w
Myog RNA (Relative Expression)